Online Calibrated, Energy-aware and Heading Corrected Pedestrian Navigation with Foot-Mounted MARG Sensors

Zebo Zhou, Zeliang Zhang, Shanhui Mo, Jin Wu, Hassen Fourati

Online Calibrated, Energy-aware and Heading Corrected Pedestrian Navigation with Foot-Mounted MARG Sensors

Zebo Zhou*, Zeliang Zhang, Shanhui Mo, Jin Wu and Hassen Fourati

Abstract:
The objective of this paper is to propose an energy-aware and ambulatory gait corrected pedestrian dead reckoning (PDR) approach using foot-mounted magnetic, angular rate and gravity (MARG) sensors. Compared with existing algorithms of PDR, the proposed method aims to solve three main problems for real pedestrian applications. First, to avoid limitations of off-line calibration for personal step length parameters, we utilize the zero-velocity-update (ZUPT) aided pedestrian MARG performance to continuously compute one's pose information. Meanwhile, it accumulates the moving distance for further estimation of one's step length during the initialization process. Secondly, due to different pedestrian gaits implicating the heading deviation angle between one's moving direction and heading, there are non-negligible impacts on pedestrian dead reckoning accuracy. The linear Kalman filter is used to recursively estimate the deviated heading during aforementioned initialization process. The third problem is related to the energy consumption. Following three aspects of adaptive energy saving work are devised: (i) energy-ware strategy for gyroscopes measurements acquisition is adopted to guarantee lower energy consumption. (ii) Modes switching mechanism of navigation computation is applied to the initialization and dead reckoning processes. (iii) De-sampling after initialization process has been invoked. Finally, real-world experiments are carried out to evaluate the performances of developed PDR system. The results show the efficiency of the suggested approach. The personal moving deviation angle obtained from the developed pedestrian navigation system can be potentially used for monitoring the patients' walking rehabilitation training and provide essential data for doctors to make constructive suggestions.

Keywords: Pedestrian Navigation, Energy Management, Kalman Filter, Heading Correction, Zero-Velocity-Update.

Z. Zhou*, Z. Zhang and S. Mo are with School of Aeronautics & Astronautics and Aircraft swarm intelligent sensing and cooperative control Key Laboratory of Sichuan Province, University of Electronic Science and Technology of China, Chengdu, China. (e-mail: klinsmann.zhou@gmail.com; zeliangzzl@163.com; rubyhui.mo@gmail.com)

J. Wu is with the Department of Electronic and Computer Engineering, Hong Kong University of Science and Technology, Hong Kong, China and is also with Tencent Robotics X, Shenzhen, China. (e-mail: jin_wu_uestc@hotmail.com; chinajinwu@tencent.com

H. Fourati is with the University Grenoble Alpes, CNRS, Inria, Gipsa-Lab, Grenoble 38400, France. (e-mail: hassen.fourati@gipsa-lab.grenoble-inp.fr)

Online Calibrated, Energy-aware and Heading Corrected Pedestrian Navigation with Foot-Mounted MARG Sensors

Abstract

The objective of this paper is to propose an energy-aware and ambulatory gait corrected pedestrian dead reckoning (PDR) approach using foot-mounted magnetic, angular rate and gravity (MARG) sensors. Compared with existing algorithms of PDR, the proposed method aims to solve three main problems for real pedestrian applications. First, to avoid limitations of off-line calibration for personal step length parameters, we utilize the zero-velocity-update (ZUPT) aided pedestrian MARG performance to continuously compute one's pose information. Meanwhile, it accumulates the moving distance for further estimation of one's step length during the initialization process. Secondly, due to different pedestrian gaits implicating the heading deviation angle between one's moving direction and heading, there are non-negligible impacts on pedestrian dead reckoning accuracy. The linear Kalman filter is used to recursively estimate the deviated heading during aforementioned initialization process. The third problem is related to the energy consumption. Following three aspects of adaptive energy saving work are devised: (i) energy-ware strategy for gyroscopes measurements acquisition is adopted to guarantee lower energy consumption. (ii) Modes switching mechanism of navigation computation is applied to the initialization and dead reckoning processes. (iii) De-sampling after initialization process has been invoked. Finally, real-world experiments are carried out to evaluate the performances of developed PDR system. The results show the efficiency of the suggested approach. The personal moving deviation angle obtained from the developed pedestrian navigation system can be potentially used for monitoring the patients' walking rehabilitation training and provide essential

data for doctors to make constructive suggestions.

Keywords: Pedestrian Navigation, Energy Management, Kalman Filter, Heading Correction, Zero-Velocity-Update.

---

1. Introduction

1.1. Motivation

Nowadays, with the increasing demands of real-time personal location based service, location-aware consumer electronics have become more and more indispensable and popular in daily life [1, 2]. Pedestrian navigation technology has been intensively studied and widely applied in numerous military and civilian applications, in particular, pedestrian localization, indoor navigation, motion capturing and body tracking [3, 4, 5, 6]. Global navigation satellite system (GNSS) provides users with satisfactory positioning accuracy in outdoor environments. However, it cannot work in GNSS challenging environments, e.g. canyons, tunnels, indoors, signal jamming or interruptions [7]. Wireless signals, e.g. Wi-Fi, Bluetooth, and ZigBee generated by local area networks have been commonly utilized as potentially feasible supplementaries through fingerprinting and trilateration for augmenting navigation solutions under those GNSS denied environments [4, 8, 9, 10]. However, the radio signals are prone to suffer from multi-path effects, e.g. signal attenuation, diffraction and refraction, thus significantly degrading the signal quality [6, 11]. Moreover, state-of-the-art ground based radio augmentation systems require a complex sensor-network infrastructure to be deployed in advance.The network system usually contains numerous beacons for good accuracy and coverage purpose such that it is neither a low-cost nor an instant-deployment solution for pedestrian navigation applications [12, 13]. Therefore, the beacon-free and self-contained navigation technology is much more preferable without any pre-installed infrastructure.

1.2. Related Work

In the past decades, with the development of micro-electro-mechanical (MEMS) technologies, MEMS inertial sensors have been extensively used for pedestrian

navigation [1, 7, 14, 15, 16].These sensors consisting of a tri-axial gyroscope and a tri-axial accelerometer are usually attached to a certain part of one's body for motion monitoring or biomedical rehabilitation purposes [17, 19, 18, 20, 21, 22]. A great deal of endeavor has been paid to improving the performances of pedestrian navigation. Existing representative methods of pedestrian navigation with inertial sensors can be mainly categorized into two sorts. One is strapdown-inertial-mechanization based method. Due to the inherent drift of gyroscopes and accelerometers, the navigation error of strapdown inertial system rapidly grows, inevitably leading to an important error [23]. To solve this problem, a considerable research on zero-velocity-update (ZUPT) method has been conducted by introducing zero velocity as a pseudo-measurement during one's stance phase of walking. It is proven to be sufficient to compensate for the inertial sensor drifts and reset the accumulation errors [24, 25, 26]. To maintain good heading accuracy and limit the vertical axis drift of gyroscope, magnetometers are increasingly common to be assembled with inertial sensors on massive low-cost devices [5, 27, 28]. It is referred to as MARG sensor that contains a triad of magnetic, angular rate and gravity components. Many researchers are concerned with magnetic disturbances and inertial drifts estimation for MARG sensor module applications [29, 30, 31, 32]. To optimally fuse data from this module, various linear and nonlinear Kalman filters (KFs) e.g. conventional KF, extended KF, unscented KF and particle KF are intensively developed to estimate the one's position and orientation [4, 27, 33, 34, 35]. The other sort of pedestrian navigation method is dead reckoning based method. It recursively integrates one's step length and orientation during each detected step. Large amount of previous studies have been performed focusing on step detection [36, 37] and step length model estimation [38, 39, 40, 41]. To further enhance the navigation accuracy and reliability, [38] developed a multi-mode pedestrian navigation algorithm by taking multi-placement of smartphones into account. More recently, multi-mode behaviors including walking, running, swing and standing still are considered as well in recent work [42]. However, the existing dead reckoning methods mentioned above need to calibrate a group of parameters with

sufficient personal off-line datasets prior to use. This is a main impediment for its being off-the-shelf product. Moreover, though various types of misalignment angles caused by inconsistency of installed sensor frame and defined body frame have been previously discussed and fixed [2, 43, 45], to the best of our knowledge, there are quite few related works discussing the heading deviation angle compensation related to personal gait in foot-mounted pedestrian navigation yet. It is worthy of mentioning that such heading deviation angle varies from persons and their gaits. Energy management is another critical issue for the wearable devices. For pedestrian navigation applications, gyroscope measurements are proven to be more reliable than accelerometers in either orientation determination or step detection [46]. However, in practice, it is universally acknowledged that the gyroscopes consume much more energy compared with accelerometers or magnetometers [47]. For instance, according to the official user manuals of STMicroelectronics, for its typical product of MEMS gyroscope LSGD20 and accelerometer LIS3DH, the former consumes about 6.1mA while the latter is merely about 11 μA [47]. On the other hand, sampling rate is also of great importance for MEMS inertial measurement unit (IMU) performances. The authors in [43] present an interesting results that a 2.5 times increase of velocity uncertainty by reducing the sampling rate from 1000 Hz to 100 Hz during ZUPT aided pedestrian inertial navigation. This strongly motivates us to develop an efficient and applicable energy saving strategy of MARG sensor module for pedestrian navigation without evidently affecting its performance.

1.3. Main Contributions

Up to now, much attention has been paid to pedestrian navigation particularly concentrating on step detection, step length modeling and sensor bias compensation but rarely with regard to efficient energy management, online pedestrian parameter calibration and gait related heading compensation. In this paper, the pedestrian navigation problem is solved under the following contributions

(1) A joint ZUPT/dead reckoning based pedestrian navigation method. It is

free of off-line calibration for personal PDR parameters. The ZUPT-aided Pedestrian MARG Navigation is utilized to continuously compute one's pose information meanwhile it accumulates the moving distance during the initialization process for further estimating one's step length in the way of dead reckoning.

(2) A gait related heading deviation angle compensation. Due to different pedestrian gaits implicating the heading deviation angle between one's moving direction and heading, there are non-negligible impacts on PDR accuracy. To solve such problem, a linear KF will be proposed to recursively estimate the deviated heading for adapting one's different behavior modes.

(3) An adaptive and efficient energy management strategy. Three aspects of adaptive energy saving work are devised: (a) Energy-aware strategy for gyroscope measurements acquisition is adopted to ensure the lower energy consumption. (b) Modes switching mechanism of navigation computation is applied to the initialization and dead reckoning processes. (c) Adaptive de-sampling during pedestrian dead reckoning process.

The proposed method has the following advantages:

(1) It is based on the energy-aware strategy thus consumes less energy.

(2) It identifies step length parameters for different users without any off-line tests.

(3) Most importantly, it adaptively corrects one's moving direction according to personal gait. Inversely, it can be potentially used for monitoring the patients' walking rehabilitation training.

1.4. Arrangement of Contents

This paper is organized as follows. In Section II, the principle and structure of proposed method is given and explained. In Section III, a gait related heading deviation angle is analyzed and compensated through a linear KF. The energy management strategy is devised in Section IV. In Section V, real experimental tests and comparisons are carried out. Finally, concluding remarks in Section VI end this paper.

2. Principle and Structure of Proposed Pedestrian Navigation Method

The overall structure of proposed pedestrian navigation method is presented in Fig. 1. It is clearly shown that two major parts are involved in pedestrian navigation computation: on-line initialization and gait based dead reckoning. During online initialization process, the ZUPT-aided pedestrian MARG navigation is performed to continuously compute one's pose information meanwhile it accumulates the moving distance to achieve on-line calibration for personal step length parameters. Besides, due to different pedestrian gaits implicating the heading deviation angle (see $\delta\gamma$ in Fig. 2) between one's moving direction and foot's heading, there are non-negligible impacts on pedestrian dead reckoning accuracy. Actually, it is not compulsory for sensor placement. If the sensor module is placed as shown in Fig. 3, the misalignment angle between forward axes of shoe and sensor can be still roughly measured by protractor beforehand. To recursively estimate the heading deviation, a linear KF is constructed. After completing initialization, the pedestrian position will be updated with dead reckoning based method. Such structure can greatly saves the computation resources than conventional ZUPT-aided inertial mechanization methods.

2.1. ZUPT-Aided Pedestrian MARG Navigation

ZUPT-aided MARG navigation not only continuously estimates ones' position, velocity and attitude (PVA) information [27, 44] , but also plays a role in initialization part for calibrating personal parameters (e.g. step length and heading deviation). At epoch k, one's PVA can be easily computed with inertial measurements through

$$\begin{cases} \boldsymbol{p}_k^{\mathrm{n}} = \boldsymbol{p}_{k-1}^{\mathrm{n}} + \boldsymbol{v}_k^{\mathrm{n}} \Delta t + \left(\boldsymbol{C}_{\mathrm{b}k}^{\mathrm{n}} \cdot \boldsymbol{f}_k + \boldsymbol{g}\right) (\Delta t)^2 / 2 \\ \boldsymbol{v}_k^{\mathrm{n}} = \boldsymbol{v}_{k-1}^{\mathrm{n}} + \left(\boldsymbol{C}_{\mathrm{b}k}^{\mathrm{n}} \cdot \boldsymbol{f}_k + \boldsymbol{g}\right) \Delta t \\ \boldsymbol{C}_{\mathrm{b}k}^{\mathrm{n}} = \boldsymbol{C}_{\mathrm{b}k-1}^{\mathrm{n}} \left(\boldsymbol{I}_3 + [\boldsymbol{\omega}_k \times] \, \Delta t\right) \end{cases} \tag{1}$$

where subscripts k and $k-1$ represent epoch indexes; superscript n and subscript b represent navigation frame (denoted as n-frame, North-East-Down) and body

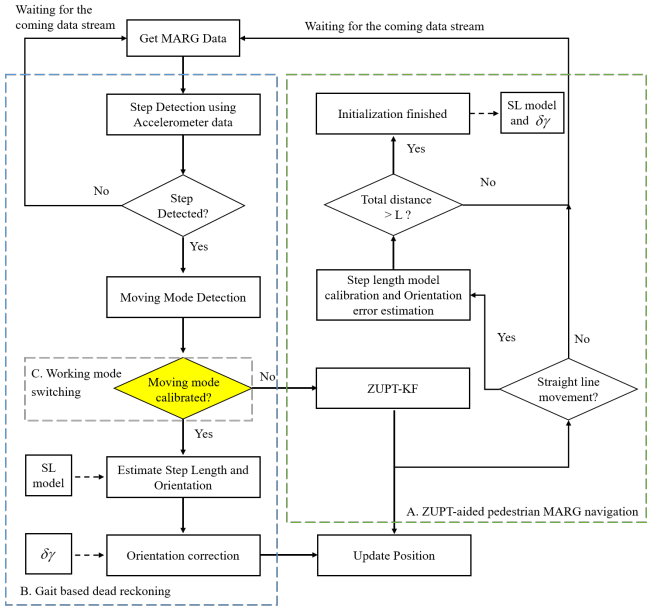

Figure 1: The diagram of proposed pedestrian navigation method

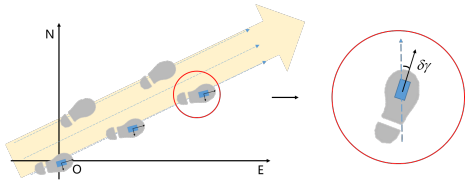

Figure 2: Illustration of pedestrian gait related heading deviation sketch (line for foot's heading; blue line for moving direction; N-E stands for 'North-East')

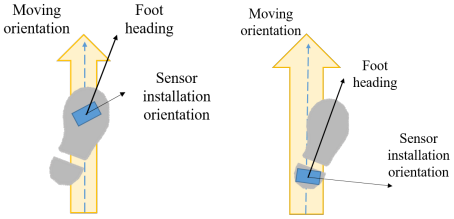

Figure 3: Two different sensor installation positions

frame (denoted as b-frame, front-right-down), respectively; $\boldsymbol{\omega}$ denotes the angular rate and $\boldsymbol{f}$ denotes the specific force; $\boldsymbol{p}$ and $\boldsymbol{v}$ are three-dimensional position and velocity vectors respectively; $\boldsymbol{C}_{\mathrm{b}}^{\mathrm{n}}$ is the direction cosine matrix transforming a vector from b-frame into n-frame; Δt denotes the sampling interval of inertial sensors; $\boldsymbol{g}$ is the local gravity vector; $\boldsymbol{I}_3$ denotes the 3 dimensional identity matrix; $[\cdot\times]$ represents the skew symmetric matrix operator.

The accelerometer and gyroscope models are established respectively as

$$\boldsymbol{y}_{\mathrm{G}} = \boldsymbol{\omega} + \boldsymbol{b}_{\mathrm{G}} + \boldsymbol{w}_{\mathrm{G}} \tag{2}$$

$$\boldsymbol{y}_{\mathrm{A}} = \boldsymbol{f} + \boldsymbol{b}_{\mathrm{A}} + \boldsymbol{w}_{\mathrm{A}} \tag{3}$$

where subscripts G and A denote the gyroscope and accelerometer respectively; $\boldsymbol{y}$ denotes the output of sensor; $\boldsymbol{w}_{\mathrm{G}}$ and $\boldsymbol{w}_{\mathrm{A}}$ are the zero mean Guassian white noises with variances $\boldsymbol{Q}_{\boldsymbol{w}_{\mathrm{G}}}$ and $\boldsymbol{Q}_{\boldsymbol{w}_{\mathrm{A}}}$ respectively; $\boldsymbol{b}_{\mathrm{G}}$ and $\boldsymbol{b}_{\mathrm{A}}$ represent the gyroscope and accelerometer biases respectively. The models of $\boldsymbol{b}_{\mathrm{G}}$ and $\boldsymbol{b}_{\mathrm{A}}$ are formulated as

$$\dot{\boldsymbol{b}}_{\mathrm{G}} = \boldsymbol{w}_{\mathrm{rG}} \tag{4}$$

$$\dot{\boldsymbol{b}}_{\mathrm{A}} = \boldsymbol{w}_{\mathrm{rA}} \tag{5}$$

where $\boldsymbol{w}_{\mathrm{rG}}$ and $\boldsymbol{w}_{\mathrm{rA}}$ are the zero mean Guassian white noises with variances $\boldsymbol{Q}_{\boldsymbol{w}_{\mathrm{rG}}}$ and $\boldsymbol{Q}_{\boldsymbol{w}_{\mathrm{rA}}}$ respectively. To limit the inertial accumulative errors, the ZUPT-aided MARG KF is constructed with the following 15-dimensional error state

$$\boldsymbol{x}^{\mathrm{I}} = \begin{bmatrix} \boldsymbol{\phi}^{\top} & \delta\boldsymbol{p}^{\top} & \delta\boldsymbol{v}^{\top} & \boldsymbol{b}_{\mathrm{G}}^{\top} & \boldsymbol{b}_{\mathrm{A}}^{\top} \end{bmatrix}^{\top} \tag{6}$$

where $\boldsymbol{\phi}$, $\delta\boldsymbol{p}$ and $\delta\boldsymbol{v}$ denote misalignment angles, position error and velocity error vectors, respectively; superscript I and II are introduced to distinguish different Kalman filters. Then the state model can be established as

$$\boldsymbol{x}_k^{\mathrm{I}} = \boldsymbol{\Phi}_{k-1,k}^{\mathrm{I}} \boldsymbol{x}_{k-1}^{\mathrm{I}} + \boldsymbol{\Gamma}_k^{\mathrm{I}} \boldsymbol{w}_k^{\mathrm{I}} \tag{7}$$

where the state transition matrix $\boldsymbol{\Phi}^{\mathrm{I}}_{k-1,k}$ and the noise transition matrix $\boldsymbol{\Gamma}^{\mathrm{I}}_{k}$ are given by

$$\boldsymbol{\Phi}^{\mathrm{I}}_{k-1,k} = \begin{bmatrix} \boldsymbol{I}_3 & \boldsymbol{0}_{3\times3} & \boldsymbol{0}_{3\times3} & -\Delta t \boldsymbol{C}^n_b & \boldsymbol{0}_{3\times3} \\ \boldsymbol{0}_{3\times3} & \boldsymbol{I}_3 & \Delta t \boldsymbol{I}_3 & \boldsymbol{0}_{3\times3} & \boldsymbol{0}_{3\times3} \\ \Delta t \left[\boldsymbol{f}^n \times \right] & \boldsymbol{0}_{3\times3} & \boldsymbol{I}_3 & \boldsymbol{0}_{3\times3} & \Delta t \boldsymbol{C}^n_b \\ \boldsymbol{0}_{3\times3} & \boldsymbol{0}_{3\times3} & \boldsymbol{0}_{3\times3} & \boldsymbol{I}_3 & \boldsymbol{0}_{3\times3} \\ \boldsymbol{0}_{3\times3} & \boldsymbol{0}_{3\times3} & \boldsymbol{0}_{3\times3} & \boldsymbol{0}_{3\times3} & \boldsymbol{I}_3 \end{bmatrix}$$

$$\boldsymbol{\Gamma}^{\mathrm{I}}_{k} = \begin{bmatrix} -\Delta t \boldsymbol{C}^n_b & \boldsymbol{0}_{3\times3} & \boldsymbol{0}_{3\times3} & \boldsymbol{0}_{3\times3} \\ \boldsymbol{0}_{3\times3} & \boldsymbol{0}_{3\times3} & \boldsymbol{0}_{3\times3} & \boldsymbol{0}_{3\times3} \\ \boldsymbol{0}_{3\times3} & \Delta t \boldsymbol{C}^n_b & \boldsymbol{0}_{3\times3} & \boldsymbol{0}_{3\times3} \\ \boldsymbol{0}_{3\times3} & \boldsymbol{0}_{3\times3} & \Delta t \boldsymbol{I}_3 & \boldsymbol{0}_{3\times3} \\ \boldsymbol{0}_{3\times3} & \boldsymbol{0}_{3\times3} & \boldsymbol{0}_{3\times3} & \Delta t \boldsymbol{I}_3 \end{bmatrix}$$

The process noise $\boldsymbol{w}^{\mathrm{I}}_{k}$ can be written as

$$\boldsymbol{w}^{\mathrm{I}}_{k} = \begin{bmatrix} \boldsymbol{w}^{\top}_{\mathrm{G}} & \boldsymbol{w}^{\top}_{\mathrm{A}} & \boldsymbol{w}^{\top}_{\mathrm{rG}} & \boldsymbol{w}^{\top}_{\mathrm{rA}} \end{bmatrix}^{\top}$$

which obeys zero mean Guassian distribution, with variance

$$\boldsymbol{Q}^{\mathrm{I}}_{k} = \mathrm{diag}\left\{ \boldsymbol{Q}_{\boldsymbol{w}_{\mathrm{G},k}}, \boldsymbol{Q}_{\boldsymbol{w}_{\mathrm{A},k}}, \boldsymbol{Q}_{\boldsymbol{w}_{\mathrm{rG},k}}, \boldsymbol{Q}_{\boldsymbol{w}_{\mathrm{rA},k}} \right\}$$

where diag represents diagonal matrix. The predicted state and its covariance matrix are computed by,

$$\boldsymbol{x}^{\mathrm{I}}_{k|k-1} = \boldsymbol{\Phi}^{\mathrm{I}}_{k-1,k} \boldsymbol{x}^{\mathrm{I}}_{k-1|k-1} \tag{8}$$

$$\boldsymbol{P}^{\mathrm{I}}_{k|k-1} = \boldsymbol{\Phi}^{\mathrm{I}}_{k-1,k} \boldsymbol{P}^{\mathrm{I}}_{k-1|k-1} \left(\boldsymbol{\Phi}^{\mathrm{I}}_{k-1,k} \right)^{\top} + \boldsymbol{\Gamma}^{\mathrm{I}} \boldsymbol{Q}^{\mathrm{I}}_{k} \left(\boldsymbol{\Gamma}^{\mathrm{I}} \right)^{\top} \tag{9}$$

Considering ZUPT and magnetic sensor output, accordingly the observation model is formulated as

$$\boldsymbol{z}^{\mathrm{I}}_{k} = \boldsymbol{H}^{\mathrm{I}}_{k} \boldsymbol{x}^{\mathrm{I}}_{k} + \boldsymbol{\varepsilon}^{\mathrm{I}}_{k} \tag{10}$$

where the observation vector $\boldsymbol{z}_k$ and the corresponding design matrix $\boldsymbol{H}_k$ are given by

$$\boldsymbol{z}^{\mathrm{I}}_{k} = \begin{bmatrix} \psi_{\mathrm{M},k} - \psi_{\mathrm{G},k} & -\boldsymbol{v}^{\top}_{k} \end{bmatrix}^{\top}$$

$$\boldsymbol{H}_k^{\mathrm{I}} = \begin{bmatrix} \boldsymbol{D} & \mathbf{0}_{1\times3} & \mathbf{0}_{1\times3} & \mathbf{0}_{1\times3} & \mathbf{0}_{1\times3} \\ \mathbf{0}_{3\times3} & \mathbf{0}_{3\times3} & \boldsymbol{I}_3 & \mathbf{0}_{3\times3} & \mathbf{0}_{3\times3} \end{bmatrix}$$

where $\psi_{\mathrm{G},k}$ denotes heading angle derived from gyroscope while $\psi_{\mathrm{M},k}$ is computed from magnetometer outputs; $\boldsymbol{D}$ is the connection matrix between misalignment angles and Euler error angles $\boldsymbol{D} = \begin{bmatrix} \sin\psi\tan\theta & -\cos\psi\tan\theta & 1 \end{bmatrix}$ (see Appendix A). The observation model noise $\boldsymbol{\varepsilon}_k^{\mathrm{I}} \sim \mathcal{N}\left(\mathbf{0}, \boldsymbol{R}_k^{\mathrm{I}}\right)$ is

$$\boldsymbol{\varepsilon}_k^{\mathrm{I}} = \begin{bmatrix} \boldsymbol{\varepsilon}_{\psi,k}^{\top} & \boldsymbol{\varepsilon}_{v,k}^{\top} \end{bmatrix}^{\top}$$

in which $\boldsymbol{\varepsilon}_{\psi,k} \sim \mathcal{N}\left(\mathbf{0}, \boldsymbol{R}_{\psi,k}\right)$ denotes the heading correction model noise; $\boldsymbol{\varepsilon}_{v,k} \sim \mathcal{N}\left(\mathbf{0}, \boldsymbol{R}_{v,k}\right)$ denotes the velocity correction model noise, which is highly determined by the static threshold setting during the zero velocity detection. The observation variance can be written as

$$\boldsymbol{R}_k = \mathrm{diag}\{\boldsymbol{R}_{\psi,k}, \boldsymbol{R}_{v,k}\}$$

Then the KF solution and its covariance are estimated by

$$\boldsymbol{x}_{k|k}^{\mathrm{I}} = \boldsymbol{x}_{k|k-1}^{\mathrm{I}} + \boldsymbol{K}_k^{\mathrm{I}}\left(\boldsymbol{z}_k^{\mathrm{I}} - \boldsymbol{H}_k^{\mathrm{I}}\boldsymbol{x}_{k|k-1}^{\mathrm{I}}\right) \tag{11}$$

$$\boldsymbol{P}_{k|k}^{\mathrm{I}} = \left(\boldsymbol{I}_{15} - \boldsymbol{K}_k^{\mathrm{I}}\boldsymbol{H}_k^{\mathrm{I}}\right)\boldsymbol{P}_{k|k-1}^{\mathrm{I}} \tag{12}$$

with the gain matrix $\boldsymbol{K}$

$$\boldsymbol{K}_k^{\mathrm{I}} = \boldsymbol{P}_{k|k-1}^{\mathrm{I}}\left(\boldsymbol{H}_k^{\mathrm{I}}\right)^{\top}\left[\boldsymbol{H}_k^{\mathrm{I}}\boldsymbol{P}_{k|k-1}^{\mathrm{I}}\left(\boldsymbol{H}_k^{\mathrm{I}}\right)^{\top} + \boldsymbol{R}_k^{\mathrm{I}}\right]^{-1} \tag{13}$$

Finally by correcting the PVA with estimated $\delta\boldsymbol{p}, \delta\boldsymbol{v}, \boldsymbol{\phi}$ and resetting error state, the ZUPT-aided MARG navigation is completed.

2.2. Gait Based Dead Reckoning

The principle of gait based dead reckoning is generally depicted as:

$$\begin{bmatrix} p_{x,k} \\ p_{y,k} \end{bmatrix} = \begin{bmatrix} p_{x,k-1} \\ p_{y,k-1} \end{bmatrix} + d_k \begin{bmatrix} \sin\gamma_k \\ \cos\gamma_k \end{bmatrix} \tag{14}$$

where $[p_{x,k}, p_{y,k}]^{\top}$ denotes the position after the k-th step ; d_k and γ_k represents the k-th step length and moving orientation respectively. For step length estimation, there are numerous models with various parameters. The most popular

one is a bi-parametric linear model [48], in which the step length is assumed to be related to the step frequency. Apart from the step frequency, other parameters are introduced into the refined step length model as well, for instance, acceleration variance [25], acceleration boundary [40], height [38] and leg length [39]. Finally, the following step length model [42] is chosen

$$\begin{cases} d_{\mathrm{W},k} = \sum_{j=0}^{2} K_j \times f_{s_k}^{-j/2} + K_3 \times \max\left(\overline{\tilde{a}}_k\right) & \text{(walking)} \\ d_{\mathrm{R},k} = K_4 \times \sqrt[3]{\overline{\tilde{a}}_k} & \text{(running)} \end{cases} \tag{15}$$

where subscripts 'W' and 'R' represent the walking and running behaviors, respectively. To remove the influences of high-frequency noise from acceleration, the Hamming-window based, linear-phase finite impulse response (FIR) filter is introduced to generate the filtered acceleration $\tilde{a}_k$. $\overline{\tilde{a}}_k$ denotes the mean value of $\tilde{a}_k$; f_{s_k} denotes step frequency during the k-th step period; K_j for $j = 0, 1, 2, 3, 4$ are coefficients that need to be calibrated beforehand. Note that the calibration can be done online during the initialization process with the given distance estimated by ZUPT-KF.

The heading angle during one motion period can be obtained based on various MARG sensors data fusion strategies [15, 38, 49]. However, the performances in real applications will be degraded due to the existence of gait related heading deviation which differs from individuals. For this reason, the heading should to be cautiously aligned to the moving direction before using (14) by

$$\gamma_i = \psi_i + \delta\gamma_i \tag{16}$$

where $\delta\gamma_i$ is the heading deviation angle between moving direction and heading; γ_i and ψ_i represent one's actual moving direction and heading angle, respectively. The compensation method for $\delta\gamma_i$ will be detailed in Section III.

2.3. Working Mode Switching

It needs to be clarified that

(i) initialization and dead reckoning are two basic working modes during pedestrian navigation.

(ii) when the changing of motion behavior is detected, the initialization mode will be triggered for performing the ZUPT-aided MARG KF and calibrating the personal parameters.

(iii) while once the initialization is successfully completed, the dead reckoning mode will be carried out with the calibrated parameters in (ii).

The working mode switching diagram is exhibited in Fig. 3. Therefore, the

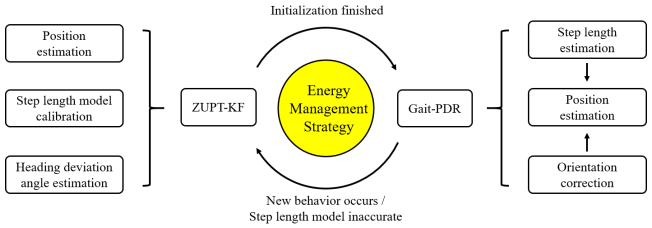

Figure 4: Diagram of working mode switching

behavior recognition is critical to detect the event of working mode switching. Here we utilize three features i.e. variance, direct component (DC) and energy to identify one's motion behaviors including walking, running, swing and standing. Based on that, the real-time state machine for multi-mode behaviors recognition is designed and developed to make decision on working mode. More details can be found in reference [42].

3. Gait Related Heading Deviation Angle Compensation

Recalling the heading deviation in (16), it has a strong relation with personal gait. Inversely, the deviation also reflects one's gait and potentially can be applied to walking rehabilitation training. As a matter of fact, personal gait has a very good repeatability thus such deviation can be estimated within aforementioned initialization period. Assuming the following state model through KF of $\dot{\delta\gamma}$ as

$$\dot{\delta\gamma}_i = \dot{\delta\gamma}_{i-1} + w_{1,i} \tag{17}$$

Letting $\boldsymbol{x}_i^{\mathrm{II}} = \begin{bmatrix} \dot{\delta\gamma}_i & \delta\gamma_i \end{bmatrix}^\top$, the state model can be reformulated as

$$\boldsymbol{x}_i^{\mathrm{II}} = \boldsymbol{\Phi}_{i-1,i}^{\mathrm{II}} \boldsymbol{x}_{i-1}^{\mathrm{II}} + \boldsymbol{w}_i^{\mathrm{II}} \tag{18}$$

where the state transition matrix $\boldsymbol{\Phi}_{i-1,i}^{\mathrm{II}}$ is

$$\boldsymbol{\Phi}_{i-1,i}^{\mathrm{II}} = \begin{bmatrix} 1 & 0 \\ \Delta t & 1 \end{bmatrix}$$

The two dimensional process noise can be written as

$$\boldsymbol{w}_i^{\mathrm{II}} = \begin{bmatrix} w_{1,i}^\top & w_{2,i}^\top \end{bmatrix}^\top$$

where $w_{1,i} \sim \mathcal{N}(\mathbf{0}, \boldsymbol{Q}_{w1})$ describes the reliability of model (17); $w_{2,i} \sim \mathcal{N}(\mathbf{0}, \boldsymbol{Q}_{w2})$ is caused by discretization of first order deviation $\dot{\delta\gamma} = \partial(\delta\gamma)/\partial t$. The variance of process noise can be written as

$$\boldsymbol{Q}^{\mathrm{II}} = \mathrm{diag}\{\boldsymbol{Q}_{w1}, \boldsymbol{Q}_{w2}\}$$

Accordingly, the observation model is established as

$$\boldsymbol{z}_i^{\mathrm{II}} = \boldsymbol{H}_i^{\mathrm{II}} \boldsymbol{x}_i^{\mathrm{II}} + \boldsymbol{\varepsilon}_i^{\mathrm{II}} \tag{19}$$

where the design matrix is $\boldsymbol{H}_i^{\mathrm{II}} = \begin{bmatrix} 0 & 1 \end{bmatrix}$ and the observation vector is constructed as $\boldsymbol{z}_i^{\mathrm{II}} = \gamma_i - \psi_i$. ψ_i denotes the heading angle obtained from ZUPT-KF, which is taken at the instant of hitting the ground. γ_i can be approximately calculated with the position increment or the velocity vector by

$$\gamma_{p,i} = \arctan \frac{\Delta p_{x,i}}{\Delta p_{y,i}} \tag{20}$$

$$\gamma_{v,i} = \arctan \frac{v_{\max x,i}}{v_{\max y,i}} \tag{21}$$

where $\begin{bmatrix} \Delta p_{x,i} & \Delta p_{y,i} \end{bmatrix}^\top$ are the two-dimensional position increment vector during the i-th step, $\begin{bmatrix} v_{\max x,i} & v_{\max y,i} \end{bmatrix}^\top$ are the maximal value of velocity during the i-th step. $\boldsymbol{\varepsilon}_i^{\mathrm{II}}$ is the zero mean Guassian noise, and its variance $\boldsymbol{R}^{\mathrm{II}}$ can be determined after obtaining the variances of heading angle and the position (or velocity). Then the deviation angle can be recursively estimated by implementing the proposed KF.

4. The Adaptive Energy Management Strategy

Three aspects of adaptive energy management (mentioned in Fig. 3) are devised including energy-aware for gyroscope, mode switching mechanism and adaptive system de-sampling.

4.1. Energy-Aware Strategy for Gyroscopes Measurements Acquisition

As is pointed out in [47], gyroscopes consume much more energy compared with that of accelerometers or magnetometers. To ensure the lower energy consumption, an energy-aware strategy for gyroscope measurements acquisition is given in Table 1.

Table 1: Energy-aware strategy for gyroscope measurements acquisition

Behavior recognition:	
IF	recognition result is non-static (e.g. "walking" or "running") ⇒ turns to **Working mode identification**
ELSE	⇒ gyroscope 'off'
Working mode identification:	
IF	working mode is "ZUPT-KF" ⇒ gyroscope 'on'
ELSE	⇒ turns to **Step length model examination**
Step length model examination:	
IF	$\Delta T_G \geq T_0$ (ΔT_G: the time interval from time instant of last step length model examination; T_0: the time duration threshold of step length model examination) ⇒ gyroscope 'on' till a whole step is completed
ELSE	⇒ gyroscope 'off'

Behavior recognition method is utilized to identify one's motion behavior and non-static behavior will wake up the gyroscope from its sleeping status. For these non-static behaviors, the gait based dead reckoning (Gait-DR) mode does not employ any gyroscope outputs while ZUPT-KF utilizes gyroscope measurements. Furthermore, one thing should be noticed that motion behavior changing may lead to corruptions of one's step length model. To avoid such

problem, without significantly increasing the computations, a periodical step length model examination procedure is introduced with a long time-interval.

4.2. Mode Switching Mechanism of Navigation Computation

Due to different computation complexity for Gait-DR and ZUPT-KF, modes switching mechanism of navigation computation mode is designed to minimize energy consumption (see Table 2).

Table 2: Mode switching mechanism of navigation computation

ZUPT-KF mode:	
Implement the following verification condition:	
IF	$L_{\mathrm{ZUPT-KF}} < L_0$
	$\Rightarrow$ keep computation mode 'ZUPT-KF'.
ELSE	$\Rightarrow$ switch the computation mode 'ZUPT-KF' to 'Gait-DR'.
Gait-DR mode:	
Implement the following verification condition:	
IF	new motion behavior is detected
	$\Rightarrow$ switch the computation mode to 'ZUPT-KF'.
ELSE IF	the step length model cannot adapt to the current motion
	$\Rightarrow$ switch the computation mode 'Gait-DR' to 'ZUPT-KF'
ELSE	$\Rightarrow$ keep 'Gait-DR' computation mode.

At the initialization stage, 'ZUPT-KF' calibrates the step length model and estimates the heading deviation angle till the accumulated moving distance $L_{\mathrm{ZUPT-KF}}$ derived from ZUPT-KF does not exceed the predetermined threshold L_0. In another word, if $L_{\mathrm{ZUPT-KF}}$ exceeds L_0, then the initialization is complete and the computation mode 'ZUPT-KF' will be switched to 'Gait-DR'. On the other hand, there are two conditions to trigger the switching 'Gait-DR' to 'ZUPT-KF': i) a new motion behavior is detected; ii) for a certain behavior, the motion frequency changes may lead to the original calibrated step length model inaccurate. For example, for running behavior, jogging and running fast are different, then one set of step length model parameters may not be incompatible with these two scenarios. Therefore, even one's motion behavior is kept, we still need to carefully monitor the possible corruption of step length model. The details of step length model examination is presented in Table 3.

Table 3: Details of step length model examination

Priori precision statistics of step length model in 'Initialization' part:
$\sigma_d = \sqrt{\frac{\sum_{i=1}^{n}(d_{\mathrm{KF},i} - d_{\mathrm{SL},i})^2}{n-1}}$
$d_{\mathrm{KF,i}}$ denotes the distance derived from ZUPT-KF at i-th step;
$d_{\mathrm{SL,i}}$ denotes the distance with calibrated step length model of i-th step
Step length model examination of 'Gait–DR':
do the examination on d_{KF} and d_{SL} with a regular time interval T_0:
by the following testing condition:
IF $\quad |d_{\mathrm{KF}} - d_{\mathrm{SL}}| \leq 3\sigma_d$
$\Rightarrow$ keep the mode 'Gait-DR'.
ELSE $\Rightarrow$ switch the mode 'Gait-DR' to 'Initialization'

4.3. Adaptive De-sampling for Gait-DR Mode

To further reduce system power consumption, an adaptive de-sampling strategy is proposed when one is with 'Gait-PDR' mode. As is widely acknowledged that, the strapdown-inertial-mechanization based method, e.g. ZUPT-KF requires a high sampling rate of inertial measurements. This is because it essentially calculates the real-time PVA information by continuous integral computation, where a lower sampling rate cannot adequately capture one's motion thus inevitably degrading the PVA accuracy. In contrast, the dead reckoning based methods calculate the position only through heading and step length of each step which only requires the sampling rate satisfying Nyquist theorem and obviously does not need a high sampling rate. Inspired by this point of view, system de-sampling is feasible to perform the pedestrian navigation during the Gait-DR working period.

5. Experimental Results and Analyses

In this section, pedestrian experiments are carried out to verify the proposed method and fully evaluate its performances. The MARG module HI229, includes accelerometers, gyroscopes and magnetometers[50]. The hardware device is mounted on one of user's foot. The module is communicated with a

memory card through TTL-USB module (Fig. 5). The computation and evaluation of proposed method is post-processed under Matlab r2015a on a Dell Inspiron14 laptop with a CPU of 4-core i5-4210U.

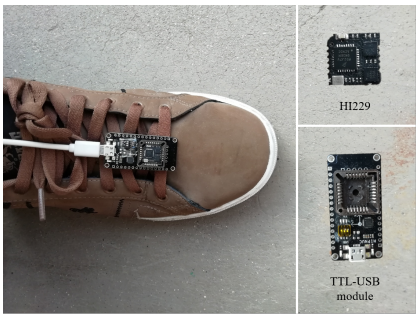

Figure 5: HI229 and TTL-USB module

As shown in Fig. 6, the octagon trajectory is designed following the corridor of report hall in the University of Electronic Science and Technology of China (UESTC) library. Three schemes are employed to estimate pedestrian trajectory for comparison purpose:

(1) ZUPT-aided pedestrian MARG navigation (ZUPT-KF)

(2) Conventional PDR based on previous offline calibration test. These methods integrates one's step length and orientation (uncorrected gait deviatation) during each detected step, such as [37, 38, 39, 40]

(3) The proposed online calibrated and heading deviation corrected Gait-PDR method.

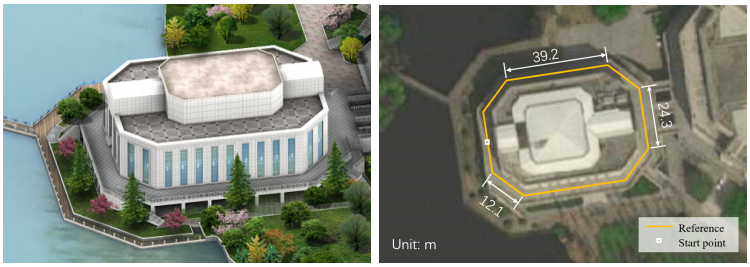

Figure 6: 2D trajectory of pedestrian experiment

To verify the accuracy of proposed method, the user is arranged to walk along the corridor of report hall twice with an arbitrary pace. For the first circular moving, ZUPT-KF is used for online calibrating step length parameter and estimating heading deviation angle which is estimated according to Section III. Then during the second circular trajactory, the working mode is switched to Gait-PDR. Fig. 7 clearly shows the heading deviation between moving direction and heading angle. γ_p and γ_v in Fig. 7 are derived from Eqs. (16) and (17) respectively. γ_p shows a better result. As a consequence, (16) is chosen in KF II to estimate heading deviation angle and the result is given in Fig. 8.

Besides, four testers' heading deviation angle estimation results are computed and presented in Table 4. Seen from this table, the gait related deviation angles are indeed varied with different persons. The largest deviation angle among testers even reaches 30 degrees. Consequently, its trajectory estimation error is much larger than others with smaller deviation angles.

Table 4: Gait related deviation angles of four testers

Testers	Gender	Age (years)	Height (cm)	Weight (kg)	Deviation angle (deg) Range	Average
Tester A	Male	24	175	65	27.5 ∼ 30.3	29.2
Tester B	Male	25	180	72	5.1∼7.1	5.8
Tester C	Female	24	158	44	15.2∼17.7	15.6
Tester D	Female	23	160	51	7.3∼9.5	8.7

For online calibration of step length model, we can point out that: to gurantee an reliable calibration process, the step frequency is used as a key indicator to discriminate different walking patterns (usually two or three patterns, i.e. walking slowly and walking fast, are adequate for describing one's walking modes). This is clearly verified through previous experiments (see Fig. 9). The threshold of step frequency variation can be empirically set as ± 0.2 according to our previous tests. Similarly, calibration in running mode also can be done in the way of calibration implemented in walking mode.

Next, we start to evaluate and compare the presented schemes, i.e. ZUPT-

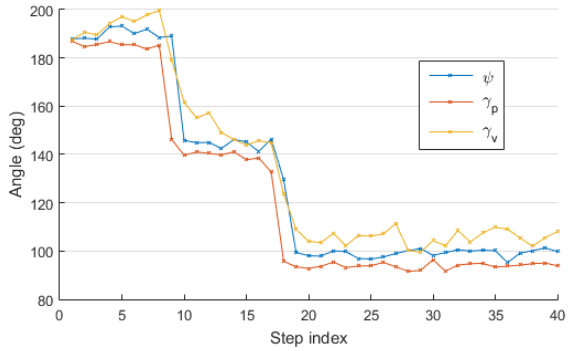

Figure 7: Comparison of moving direction and heading (walking)

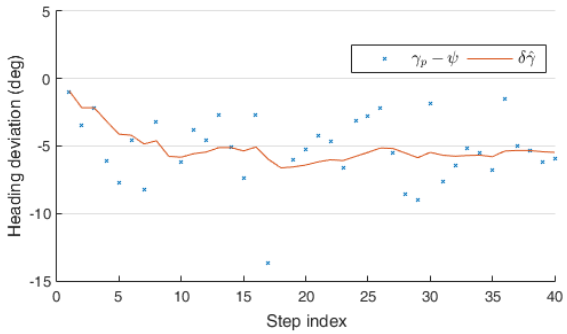

Figure 8: Gait related heading deviation angle estimation results (walking)

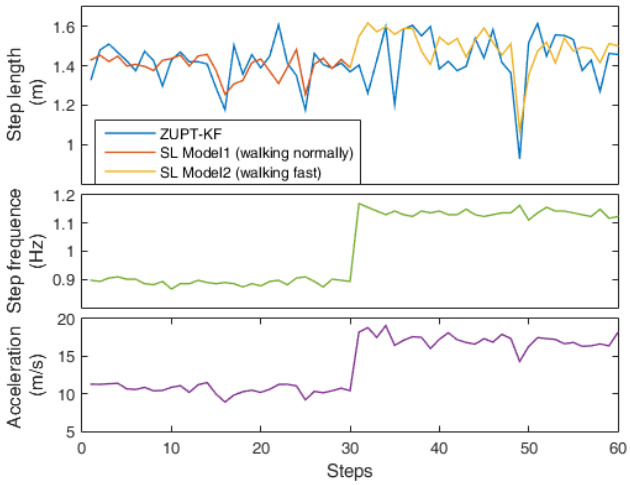

Figure 9: Step features of walking normally and walking fast

KF, PDR and Gait-PDR with the data of second cycle trajectory (shown in Fig. 10). The reference trajectory is obtained with a distance-measuring tape. The default sampling rate is set as 200Hz. With this high sampling rate, both ZUPT-KF and Gait-PDR methods perform well, while PDR method is inferior to ZUPT-KF and Gait-PDR suffering from the heading deviation angle. Comparisons of de-sampling cases are shown in Fig. 11. Result shows that Gait-PDR method maintains a good performance even at a lower sampling rate. In contrast, ZUPT-KF method gradually works worse even diverges as the sampling rate decreases as a result of sparse inertial integral computations. We also

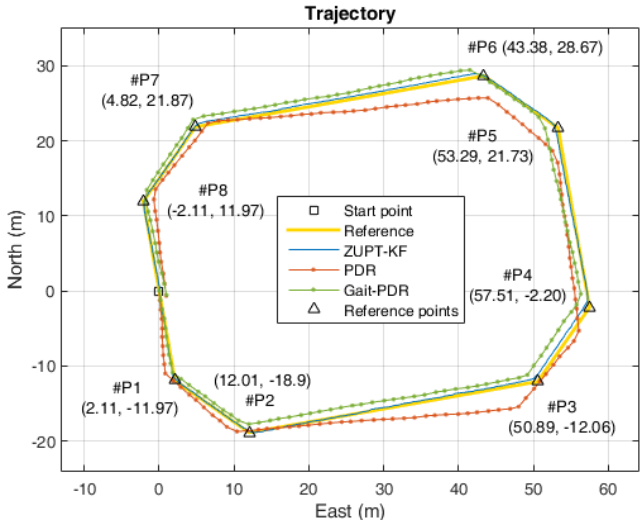

Figure 10: Trajectory comparisons of different methods (walking with the sampling rate of 200Hz)

verify these three schemes in the running scenario. The trajectory results are drawn in Fig. 10 ∼12. Compared to Fig. 8, Fig. 12 shows that for the same test, heading deviation angles for different behaviors may be different.

More detailed errors evaluation in walking and running experiments are listed in Table 5. It needs to be clarified that the average time consumption criterion of one step is computed based on the number of total steps and their

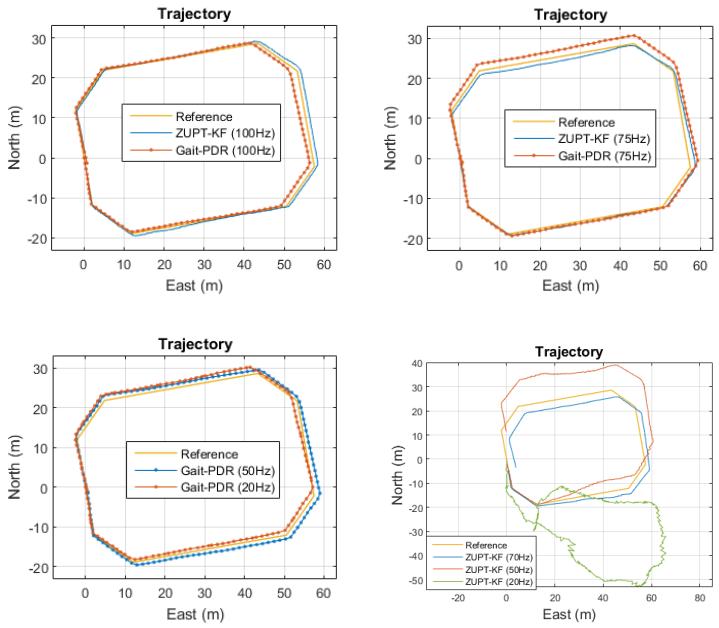

Figure 11: Results of de-sampling cases (walking)

time consumptions. The relative error of distance is defined as

$$\sigma_d = \frac{\left|\hat{d}_{\text{tol}} - d_{\text{ref}}\right|}{d_{\text{ref}}} \times 100\% \tag{22}$$

where d_{ref} is the reference distance; $\hat{d}_{\text{tol}}$ is the total distance derived from ZUPT-KF or Gait-PDR methods. The position error of starting point is obtained according to the closure trajectory. Besides, the position accuracy and maximum heading deviation are also given for comparison purpose. Since the 'ground-truth' position of each step cannot be acquired, the position uncertainty is evaluated by feature points consisting of eight corner points $\#\text{P}k\,(k = 1, 2, \ldots, 8)$ and the end point #P9. The positions of these points (as shown in Fig.10) are utilized as references to compute the root mean square error (RMSE) of horizontal position through

$$\text{RMSE}\,(p) = \frac{1}{N}\sum_{k=1}^{N}\sqrt{\left(p_{\text{ref},x,k} - \hat{p}_{x,k}\right)^2 + \left(p_{\text{ref},y,k} - \hat{p}_{y,k}\right)^2} \tag{23}$$

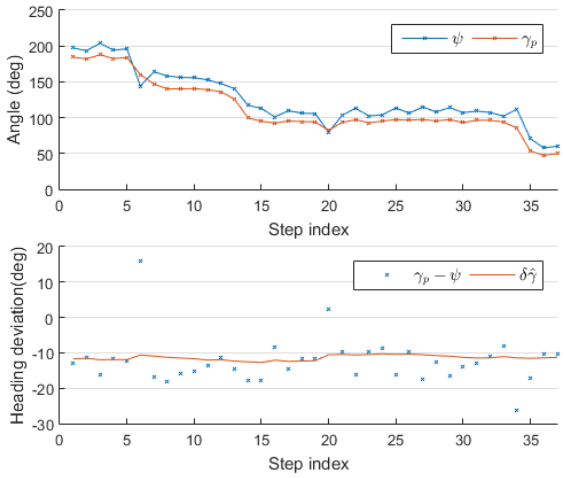

Figure 12: Gait related heading deviation angle estimation results (running)

where $N = 9$ denotes the number of referenced (subscript 'ref') feature points. These results statistics are fully consistent with the advantages and disadvantages of listed methods. Furthermore, for the aspect of energy saving, Table 5 also provides the average time consumptions for ZUPT-KF and Gait-PDR methods. Results show that Gait-PDR generally consumes much less time compared with ZUPT-KF in all cases of sampling rate. In particular, with sampling rate of 200Hz, time consumptions of ZUPT-KF and Gait-PDR in walking mode are 100.4ms and 23.8ms respectively; for running, their time consumptions are 78.0ms and 15.7ms respectively. As sampling rate decreases, time consumptions of these two methods are both significantly reduced. However, de-sampling rate leads to large errors on ZUPT-KF even divergence. Concretely speaking, as sampling rate decreases from 200Hz to 50Hz for walking mode, the time consumption of ZUPT-KF is minimized from 100.4ms to 24.9ms, while its trajectory misclosure is enlarged from 0.1m to 11.6m. It is also noticed that the max orientation errors of ZUPT-KF is significantly amplified when sampling rate decreases. This is mainly caused by non-commutativity of the rotation operations [51]. By contrast, our proposed Gait-PDR is insensitive to sampling rate (the trajectory misclosure errors are 1.1m and 1.6m for 200Hz and 20 Hz

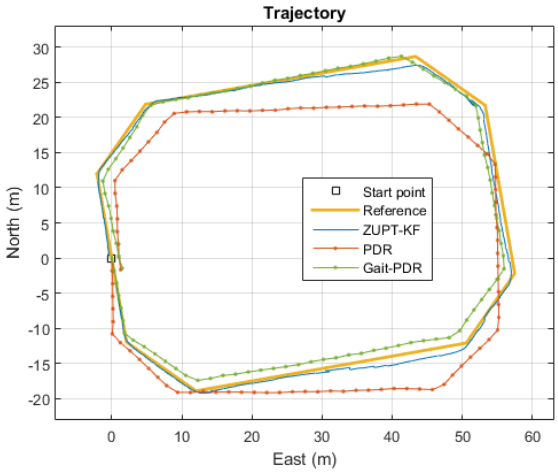

Figure 13: Trajectory comparisons of different methods (running with the sampling rate of 200Hz)

respectively). Table 6 presents the gait deviation influences imposing on position accuracies of four testers under a given testing scenario. Once again, the results show that the deviation angle has non-negligible impacts on pedestrian dead reckoning and our deviation angle compensation method is effective in improving the position accuracy. The total distance error is given in Table 7. It intuitively shows the influence of de-sampling on two methods. Thus conventional ZUPT-KF is not suitable for the platform with low sampling rate. One the contrary, Gait-PDR is very computationally efficient compared with ZUPT-KF. Meanwhile it still maintains a good accuracy even in the scenarios of low sampling rate. It is therefore very promising for its calibration convenience (online), computation efficiency and high accuracy in future wearable consumer electronics devices.

To verify the mode switching mechanism and gyroscopes energy-ware strategy, the users are allowed to walk or run in their own paces to collect a new dataset. Behaviors identification and working mode switching results are shown in Fig. 15. It shows gyroscope is only employed in initialization process and also used to examine step length model in Gait-PDR mode. It is switched off

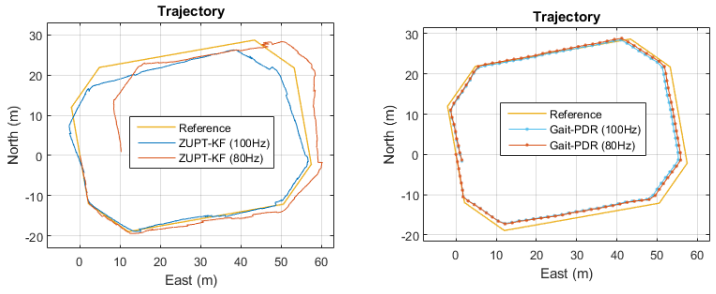

Figure 14: Results of de-sampling cases (running)

for energy saving purpose in the rest time.

There are three key factors related to power consumption, i.e. communication, computational complexity and execution time. Usually power consumption of system can hardly be accurately quantized with the first factor. It is universally known that communication cost is highly related to sampling rate of hardware system. Therefore, qualitatively speaking, our method with a lower sampling rate inevitably consumes much less power than ZUPT-KF method. The second factor is also a common indicator to reflect the system power consumption. To clearly show the computational complexity difference between two methods, an example is given as follows:

Given matrix A with dimension of $m \times n$ and B with dimension of $n \times p$, the computation complexity of $A \times B$ is defined as

$$T\left(A_{m\times n} \times B_{n\times p}\right) = O(m \times n \times p) \tag{24}$$

Table 8 presents complexity comparison between ZUPT-KF and PDR during one step walking period where zero velocity lasts about 0.3 seconds. Actually, after successfully initializing, our proposed method reduces to PDR method. It is obviously superior to ZUPT-KF method in aspect of computation complexity. Next we focus on the computation of initialization which contains two main parts: step length model calibration and heading deviation correction. The whole computation complexity for one time of initialization in our method consumes $O(88n)$, where n denotes the counting number of steps during the

Table 5: Statistics results for pedestrian navigation accuracy and time consumption

Behavior	Working mode	Sampling (Hz)	Average time consumption for one step ($\times 10^{-3}$ s)	Distance relative error	Misclosure (m)	RMSE (p) (m)	Max orientation error (deg)
Walking	ZUPT-KF	200	100	0.57%	0.10	0.46	0.9
		100	48	1.10%	0.45	0.59	1.2
		75	36	0.80%	0.51	0.89	3.0
		70	33	0.57%	5.31	3.12	3.1
		50	24	5.30%	11.60	8.95	7.1
	Gait-PDR	200	23	0.57%	1.13	1.50	1.1
		100	12	0.59%	1.51	1.28	1.3
		75	6	0.59%	1.11	1.42	1.6
		50	4	0.57%	1.56	1.21	1.6
		20	2	0.58%	1.61	1.39	2.0
Running	ZUPT-KF	200	78	1.46%	0.51	0.65	1.4
		100	42	3.06%	4.37	2.67	9.9
		80	35	3.18%	10.35	5.65	10.1
	Gait-PDR	200	16	2.01%	1.16	1.73	1.4
		100	7	2.64%	2.21	1.78	1.6
		80	6	3.46%	2.00	1.87	1.6

initialization. Supposing n as 40, the computation complexity of one time of initialization is $O(3520)$. It should be pointed out that the times of initialization is limited and usually does not exceed $3 \sim 5$ considering one's typical motion behavior modes. Therefore, likewise, our proposed method has a power-consuming advantage on computation complexity.

Intuitively, the last factor has the most straightforward connection with power consumption. The average time consumption of one step is presented in Table

Table 6: Gait deviation influences imposing on position accuracies of four testers with sampling rate of 100Hz (unit: m)

Testers	RMSE(p): PDR	RMSE(p): Gait-PDR
Tester A	20.34	1.34
Tester B	4.10	1.28
Tester C	10.26	1.15
Tester D	7.28	1.30

Table 7: Total distance error (walking)

Working mode	Sampling (Hz)	Total distance error (m)
ZUPT-KF	200	1.00
	50	9.29
Gait-PDR	200	1.00
	50	1.01

Table 8: Complexity comparison between ZUPT-KF and PDR during walking period of 1.2 seconds

Method	Sampling rate (Hz)	Computation cycles	Complexity
ZUPT-KF	200	60	$O(1.0377 \times 10^6)$
PDR	50	1	$O(6)$

9. Owing to the mode switching mechanism and de-sampling strategy, the consumed time of proposed method in one step is reduced by 80.75%. Therefore, considering overall facts above, we cautiously come to a conclusion that our proposed method outperforms the ZUPT-KF method for power consumption.

To further verify the proposed online calibrated step length model, the representative step length models with offline calibration are compared with our step length model with online calibrated parameters [52, 53, 54, 55]. The estimated step length results are presented in Fig. 16. It is obvious that the proposed method is much more accurate and reliable than others especially when undergoing transitions of different behaviors.

Table 9: Average time consumption for one step

Method	Time Consumption ($\times 10^{-3}$ s)
ZUPT-KF (200Hz)	104
Proposed method	**20**

6. Conclusion

In this paper, an online calibrated, energy-aware and ambulatory gait corrected pedestrian dead reckoning (Gait-PDR) method is proposed for pedestrian navigation via the foot-mounted magnetic, angular rate and gravity (MARG)

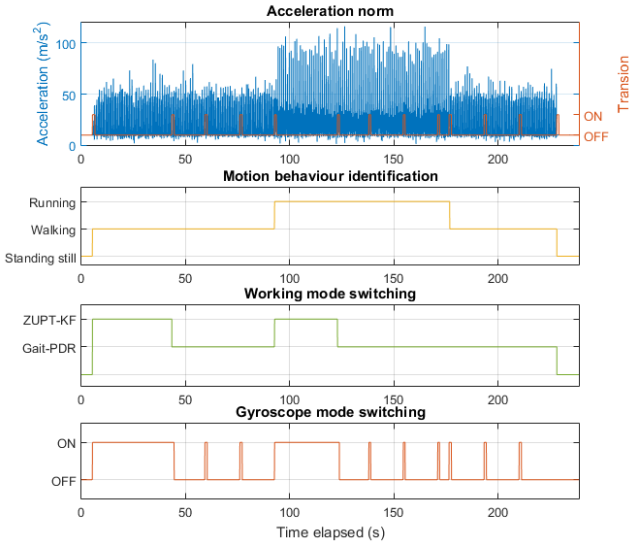

Figure 15: Illustrations of behaviors identification, working mode switching and gyroscope mode switching.

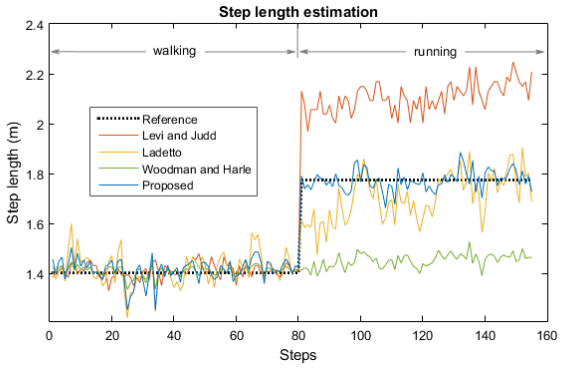

Figure 16: Step length estimation results in the scenario of behaviors transition

sensors. The proposed method solves three main problems for current pedestrian navigation applications: online calibration, gait related heading deviation and adaptive energy management. The real pedestrian experiments are carried out to demonstrate the validity and efficiency of proposed method. The results show that this latter outperforms the representative methods especially for low sampling rate scenarios. Overall, it is accurate, energy-saving and easy-to-implement thus is very promising for pedestrian navigation applications. In addition, the personal deviation angle obtained during the pedestrian navigation process would be an essential indicator for evaluating the efficiency of patients' walking rehabilitation training. In the future, more complex pedestrian behavior modes e.g. going upstairs, downstairs and climbing will be extended in theory.

Appendix A

Due to the existence of sensor error, there is a small difference between 'true' attitude matrix $\boldsymbol{C}_{\mathrm{b}}^{\mathrm{n}}$ and the estimated one $\boldsymbol{C}_{\mathrm{b}}^{\mathrm{n}'}$ (n and n$'$ represent the 'true' navigation frame and calculated navigation frame). According to the chain rule of coordinate frame,

$$\boldsymbol{C}_{\mathrm{b}}^{\mathrm{n}} = \boldsymbol{C}_{\mathrm{n}'}^{\mathrm{n}} \boldsymbol{C}_{\mathrm{b}}^{\mathrm{n}'} \tag{25}$$

where $\boldsymbol{C}_{\mathrm{n}}^{\mathrm{n}'}$ is defined as misalignment attitude matrix and it is very close to identity matrix. Therefore it can be written as:

$$\begin{aligned} \boldsymbol{C}_{\mathrm{n}'}^{\mathrm{n}} &= \boldsymbol{I}_3 + [\boldsymbol{\phi}\times] \\ &= \begin{bmatrix} 1 & -\phi_z & \phi_y \\ \phi_z & 1 & -\phi_x \\ -\phi_y & \phi_x & 1 \end{bmatrix} \end{aligned} \tag{26}$$

in which $\boldsymbol{\phi}$ is referred to as misalignment angle. Herein, the rotation matrix $\boldsymbol{C}_{\mathrm{n}}^{\mathrm{b}}$ can be expressed a set of Euler angles

$$\boldsymbol{C}_{\mathrm{n}}^{\mathrm{b}} = \begin{bmatrix} \mathrm{c}_\beta \mathrm{c}_\psi - \mathrm{s}_\beta \mathrm{s}_\theta \mathrm{s}_\psi & \mathrm{s}_\psi \mathrm{c}_\beta + \mathrm{c}_\psi \mathrm{s}_\beta \mathrm{s}_\theta & -\mathrm{s}_\beta c_\theta \\ -\mathrm{c}_\theta \mathrm{s}_\psi & \mathrm{c}_\theta \mathrm{c}_\psi & \mathrm{s}_\theta \\ s_\beta \mathrm{c}_\psi + \mathrm{c}_\beta \mathrm{s}_\theta \mathrm{s}_\psi & \mathrm{s}_\psi \mathrm{s}_\beta - \mathrm{c}_\beta \mathrm{s}_\theta \mathrm{c}_\psi & \mathrm{c}_\theta \mathrm{c}_\beta \end{bmatrix} \tag{27}$$

where the Euler angles are with the rotation order of '3-1-2', i.e. yaw-pitch-roll ($\psi - \theta - \beta$); c and s denote cosine and sine functions respectively. Denoting the calculated Euler angles as $\begin{bmatrix} \psi' & \theta' & \beta' \end{bmatrix}^\top$, and then the Euler angle errors are

$$\begin{bmatrix} \delta\psi \\ \delta\theta \\ \delta\beta \end{bmatrix} = \begin{bmatrix} \psi' \\ \theta' \\ \beta' \end{bmatrix} - \begin{bmatrix} \psi \\ \theta \\ \beta \end{bmatrix} \tag{28}$$

Knowing $\boldsymbol{C}_{\mathrm{b}}^{\mathrm{n}} = \left(\boldsymbol{C}_{\mathrm{n}}^{\mathrm{b}}\right)^\top$ and inserting (26) (27) (28) into (25), we have

$$\begin{bmatrix} \delta\psi \\ \delta\theta \\ \delta\beta \end{bmatrix} = \frac{1}{c_\theta} \begin{bmatrix} s_\psi s_\theta & -c_\psi s_\theta & c_\theta \\ -c_\psi c_\theta & -s_\psi c_\theta & 0 \\ s_\psi & -c_\psi & 0 \end{bmatrix} \begin{bmatrix} \phi_x \\ \phi_y \\ \phi_z \end{bmatrix} \tag{29}$$

Thereby the heading errors is written as

$$\delta\psi = \boldsymbol{D}\boldsymbol{\phi} \tag{30}$$

where $\boldsymbol{D} = \begin{bmatrix} \mathrm{sin}\psi\mathrm{tan}\theta & -\mathrm{cos}\psi\mathrm{tan}\theta & 1 \end{bmatrix}$ is only related to heading and pitch angles.

Acknowledgements

This work was supported by the National Natural Science Foundation of China (42074038) and the Department of Science and Technology of Sichuan Province (2021YJ0104).

References

[1] J. B. Bancroft and G. Lachapelle, "Estimating MEMS Gyroscope g-Sensitivity Errors in Foot Mounted Navigation," in *IEEE UPINLBS*. IEEE, 2012, pp. 1–6.

[2] L.-F. Shi, Y.-L. Zhao, G.-X. Liu, S. Chen, Y. Wang, and Y.-F. Shi, "A Robust Pedestrian Dead Reckoning System Using Low-Cost Magnetic and Inertial Sensors," *IEEE Trans. Instrum. Meas.*, vol. 68, no. 8, pp. 2996–3003, Aug 2019.

[3] Y. Jin, H.-S. Toh, W.-S. Soh, and W.-C. Wong, "A Robust Dead-Reckoning Pedestrian Tracking System with Low Cost Sensors," in *IEEE PERCOM*. IEEE, 2011, pp. 222–230.

[4] Q. Tian, K. I.-K. Wang, and Z. Salcic, "A Low-Cost INS and UWB Fusion Pedestrian Tracking System," *IEEE Sensors J.*, vol. 19, no. 10, pp. 3733–3740, May 2019.

[5] H. Wang, L. Cong, and H. Qin, "A Real-Time Pedestrian Dead Reckoning System With FM-Aided Motion Mode Recognition," *IEEE Sensors J.*, vol. 19, no. 8, pp. 3020–3032, Apr 2019.

[6] X. Tong, Y. Su, Z. Li, C. Si, G. Han, J. Ning, and F. Yang, "A Double-Step Unscented Kalman Filter and HMM-Based Zero-Velocity Update for Pedestrian Dead Reckoning Using MEMS Sensors," *IEEE Trans. Indust. Elect.*, vol. 67, no. 1, pp. 581–591, Jan 2020.

[7] Q. Fan, H. Zhang, P. Pan, X. Zhuang, J. Jia, P. Zhang, Z. Zhao, G. Zhu, and Y. Tang, "Improved Pedestrian Dead Reckoning Based on a Robust Adaptive Kalman Filter for Indoor Inertial Location System," *Sensors*, vol. 19, no. 2, pp. 294, 2019.

[8] Y. Gu, C. Zhou, A. Wieser, and Z. Zhou, "Trajectory Estimation and Crowdsourced Radio Map Establishment from Foot-Mounted IMUs, Wi-Fi Fingerprints, and GPS Positions," *IEEE Sensors J.*, vol. 19, no. 3, pp. 1104–1113, 2019.

[9] U. Steinhoff and B. Schiele, "Dead Reckoning from the Pocket - An Experimental Study," *IEEE PERCOM*, Mar 2010.

[10] Q. Liang and M. Liu, "An Automatic Site Survey Approach for Indoor Localization Using a Smartphone," *IEEE TASE*, vol. 17, no. 1, pp. 191–206, 2020.

[11] J.-O. Nilsson, D. Zachariah, I. Skog, and P. Händel, "Cooperative Localization by Dual Foot-Mounted Inertial Sensors and Inter-Agent Ranging," *EURASIP J. Adv. Signal Process.*, vol. 2013, no. 1, Oct 2013.

[12] G. Piccinni, G. Avitabile, and G. Coviello, "An Improved Technique based on Zadoff-Chu Sequences for Distance Measurements," *IEEE RADIO*, Oct 2016.

[13] G. Piccinni, G. Avitabile, G. Coviello, "A Novel Distance Measurement Technique for Indoor Positioning Systems based on Zadoff-Chu Sequences," *IEEE NEWCAS*, Jun 2017.

[14] C. M. Brahms, Y. Zhao, D. Gerhard, and J. M. Barden, "Stride Length Determination during Overground Running Using a Single Foot-Mounted Inertial Measurement Unit," *J. Biomechanics*, vol. 71, pp. 302–305, 2018.

[15] R. Valenti, I. Dryanovski, and J. Xiao, "Keeping a good attitude: A quaternion-based orientation filter for imus and margs," *Sensors*, vol. 15, no. 8, pp. 19 302–19 330, Aug 2015.

[16] X. Meng, Z. Q. Zhang, J. K. Wu, W. C. Wong, and H. Yu, "Self-contained pedestrian tracking during normal walking using an inertial/magnetic sensor module," *IEEE Trans. Biomed. Eng.*, vol. 61, no. 3, pp. 892–899, 2014.

[17] G. V. Prateek, I. Skog, M. E. McNeely, R. P. Duncan, G. M. Earhart, and A. Nehorai, "Modeling, Detecting, and Tracking Freezing of Gait in Parkinson Disease Using Inertial Sensors," *IEEE Trans. Biomed. Eng.*, vol. 65, no. 10, pp. 2152–2161, Oct 2018.

[18] D. Trojaniello, A. Cereatti, and U. D. Croce, "Foot Clearance Estimation during Overground Walking and Vertical Obstacle Passing using Shank-Mounted MIMUs in Healthy and Pathological Subjects," *IEEE EMBC*, Aug 2015.

[19] A. Gómez-Espinosa, N. Espinosa-Castillo, and B. Valdés-Aguirre, "Foot-Mounted Inertial Measurement Units-Based Device for Ankle Rehabilitation," *Applied Sciences*, vol. 8, no. 11, pp. 2032, 2018.

[20] Y. Ma, Z. E. Ashari, M. Pedram, N. Amini, D. Tarquinio, K. Nouri-Mahdavi, M. Pourhomayoun, R. D. Catena, and H. Ghasemzadeh, "Cyclepro: A Robust Framework for Domain-Agnostic Gait Cycle Detection," *IEEE Sensors J.*, vol. 19, no. 10, pp. 3751–3762, 2019.

[21] K. Turcot, R. Aissaoui, K. Boivin, M. Pelletier,N. Hagemeister, and J.A. De Guise, "New accelerometric method to discriminate between asymptomatic subjects and patients with medial knee osteoarthritis during 3-D gait," *IEEE Trans. Biomed. Eng.*, vol. 55, no. 4, pp. 1415–1422, 2008.

[22] A. Rampp, J. Barth, and S. Sch ulein, " Inertial Sensor Based Stride Parameter Calculation from Gait Sequences in Geriatric Patients," *IEEE Trans. Biomed. Eng.*, In press(4), pp. 1–8, 2014.

[23] E. Foxlin, "Pedestrian Tracking with Shoe-Mounted Inertial Sensors," *IEEE Computer Graphics and Applications*, vol. 25, no. 6, pp. 38–46, 2005.

[24] A. R. Jiménez, F. Seco, J. C. Prieto, and J. Guevara, "Indoor Pedestrian Navigation Using an INS/EKF Framework for Yaw Drift Reduction and a Foot-Mounted IMU," in *2010 7th Workshop on Positioning, Navigation and Communication*. IEEE, 2010, pp. 135–143.

[25] R. Zhang, H. Yang, F. Hoflinger, and L. M. Reindl, "Adaptive Zero Velocity Update Based on Velocity Classification for Pedestrian Tracking," *IEEE Sensors J.*, vol. 17, no. 7, pp. 2137–2145, Apr 2017.

[26] J. Wahlstrom, I. Skog, F. Gustafsson, A. Markham, and N. Trigoni, "Zero-Velocity Detection—A Bayesian Approach to Adaptive Thresholding," *IEEE Sensors Lett.*, vol. 3, no. 6, pp. 1–4, Jun 2019.

[27] J.-O. Nilsson, A. K. Gupta, and P. Handel, "Foot-Mounted Inertial Navigation Made Easy," *IEEE IPIN*, Oct 2014.

[28] H. Fourati, "Heterogeneous Data Fusion Algorithm for Pedestrian Navigation via Foot-Mounted Inertial Measurement Unit and Complementary Filter," *IEEE Trans. Instrum. Meas.*, vol. 64, no. 1, pp. 221–229, 2015.

[29] J. Wu, Z. Zhou, X. Zhang, M. Chen, and P. Shao, "Real-time Magnetic disturbance Determination for Micro Air Vehicles via Gravity and Global Navigation Satellite System Measurements," *Meas. Sci. Tech.*, vol. 30, no. 2, 2019.

[30] R. Jirawimut, P. Ptasinski, V. Garaj, F. Cecelja, and W. Balachandran, "A Method for Dead Reckoning Parameter Correction in Pedestrian Navigation System," *IEEE Trans. Instrum. Meas.*, vol. 52, no. 1, pp. 209–215, 2003.

[31] D. Roetenberg, H. Luinge, C. Baten, and P. Veltink, "Compensation of Magnetic Disturbances Improves Inertial and Magnetic Sensing of Human Body Segment Orientation," *IEEE Trans. Neural Syst. Rehabili. Eng.*, vol. 13, no. 3, pp. 395–405, Sep 2005.

[32] J. Wu, "MARG Attitude Estimation Using Gradient-Descent Linear Kalman Filter," *IEEE TASE*, vol. 7, no. 4, pp. 1777–1790, Oct. 2020.

[33] X. Xu, M. Wang, L. Luo, Z. Meng, and E. Wang, "An Indoor Pedestrian Localization Algorithm Based on Multi-Sensor Information Fusion," *J. Comput. Commun.*, vol. 05, no. 03, pp. 102–115, 2017.

[34] Y. Wu, H. Zhu, Q. Du, and S. Tang, "A Pedestrian Dead-Reckoning System for Walking and Marking Time Mixed Movement Using an SHSs Scheme and a Foot-Mounted IMU," *IEEE Sensors J.*, vol. 19, no. 5, pp. 1661–1671, Mar 2019.

[35] H. Xia, J. Zuo, S. Liu, and Y. Qiao, "Indoor Localization on Smartphones Using Built-In Sensors and Map Constraints," *IEEE Trans. Instrum. Meas.*, vol. 68, no. 4, pp. 1189–1198, Apr 2019.

[36] H. Guo, M. Uradzinski, H. Yin, and M. Yu, "Indoor Positioning based on Foot-Mounted IMU," *Bulletin Polish Acad. Sci. Tech. Sci.*, vol. 63, no. 3, pp. 629–634, 2015.

[37] A. R. Jimenez, F. Seco, C. Prieto, and J. Guevara, "A Comparison of Pedestrian Dead-Reckoning Algorithms Using a Low-Cost MEMS IMU," in *IEEE ISISP*. IEEE, 2009, pp. 37–42.

[38] Q. Tian, Z. Salcic, K. I.-K. Wang, and Y. Pan, "A Multi-Mode Dead Reckoning System for Pedestrian Tracking Using Smartphones," *IEEE Sensors J.*, vol. 16, no. 7, pp. 2079–2093, Apr 2016.

[39] K.-C. Lan and W.-Y. Shih, "Using Smart-Phones and Floor Plans for Indoor Location Tracking-Withdrawn," *IEEE Trans. Human Mach. Syst.*, vol. 44, no. 2, pp. 211–221, 2014.

[40] N.-H. Ho, P. Truong, and G.-M. Jeong, "Step-Detection and Adaptive Step-Length Estimation for Pedestrian Dead-Reckoning at Various Walking Speeds Using a Smartphone," *Sensors*, vol. 16, no. 9, pp. 1423, Sep 2016.

[41] H. Zhang, W. Yuan, Q. Shen, T. Li, and H. Chang, "A Handheld Inertial Pedestrian Navigation System With Accurate Step Modes and Device Poses Recognition," *IEEE Sensors J.*, vol. 15, no. 3, pp. 1421–1429, Mar 2015.

[42] Z. Zhou, S. Mo, J. Wu, and H. Fourati, "Behaviors Classification based Distance Measuring System for Pedestrians via a Foot Mounted Inertial Sensor," *Asian J. Control*, vol. 21, no. 4, pp. 1483–1495, Dec 2018.

[43] Y. Wang, A. Chernyshoff, and A. M. Shkel, "Error Analysis of ZUPT-Aided Pedestrian Inertial Navigation," *IEEE IPIN*, Sep 2018.

[44] J-O. Nilsson, I. Skog, P. Händel, and K.V.S. Hari, "Foot-mounted INS for Everybody - An Open-source Embedded Implementation, "*IEEE PLANS*, Apr 2012.

[45] A. Manos, I. Klein, and T. Hazan, "Gravity-Based Methods for Heading Computation in Pedestrian Dead Reckoning," *Sensors*, vol. 19, no. 5, pp. 1170, Mar 2019.

[46] W. Zhang, D. Wei, and H. Yuan, "Novel Drift Reduction Methods in Foot-Mounted PDR System," *Sensors*, vol. 19, no. 18, pp. 3962, Sep 2019.

[47] A. Makni, H. Fourati, and A. Y. Kibangou, "Energy-Aware Adaptive Attitude Estimation under External Acceleration for Pedestrian Navigation," *IEEE/ASME Trans. Mech.*, vol. 21, no. 3, pp. 1366–1375, 2015.

[48] Z. Sun, X. Mao, W. Tian, and X. Zhang, "Activity Classification and Dead Reckoning for Pedestrian Navigation with Wearable Sensors," *Meas. Sci. Tech.*, vol. 20, no. 1, pp. 015203, Nov 2008.

[49] R. Stirling, K. Fyfe, and G. Lachapelle, "Evaluation of a New Method of Heading Estimation for Pedestrian Dead Reckoning Using Shoe Mounted Sensors," *J. Navigation*, vol. 58, no. 1, pp. 31–45, Jan 2005.

[50] Beijing Beyond Core Electronic Technology Co., Ltd. HI229. Available: https://yandld.gitee.io/product_doc/.

[51] S. Stančin, and S. Tomažič, "Angle estimation of simultaneous orthogonal rotations from 3D gyroscope measurements," *Sensors*, vol. 11, no. 9, pp. 8536–8549, Aug 2011.

[52] R. W. Levi and T. Judd, "Dead Reckoning Navigational System Using Accelerometer to Measure Foot Impacts," 1996, uS Patent 5,583,776.

[53] Q. Ladetto, "On Foot Navigation: Continuous Step Calibration Using both Complementary Recursive Prediction and Adaptive Kalman Filtering," in *Proceedings of ION GPS*, vol. 2000, 2000, pp. 1735–1740.

[54] O. Woodman and R. Harle, "Pedestrian Localisation for Indoor Environments," in *Proceedings of the 10th international conference on Ubiquitous computing*, 2008, pp. 114–123.

[55] B. Krach and P. Roberston, "Cascaded Estimation Architecture for Integration of Foot-Mounted Inertial Sensors," in *IEEE PLANS*. IEEE, 2008, pp. 112–119.